

Saving superconducting quantum processors from qubit decay and correlated errors generated by gamma and cosmic rays

John M. Martinis¹

¹*Quantala, Santa Barbara, CA 93105, USA**
(Dated: December 22, 2024)

Error-corrected quantum computers can only work if errors are small and uncorrelated. Here I show how cosmic rays or stray background radiation affects superconducting qubits by modeling the phonon to electron/quasiparticle down-conversion physics. For present designs, the model predicts about 57% of the radiation energy breaks Cooper pairs into quasiparticles, which then vigorously suppress the qubit energy relaxation time ($T_1 \sim 160$ ns) over a large area (cm) and for a long time (ms). Such large and correlated decay kills error correction. Using this quantitative model, I show how this energy can be channeled away from the qubit so that this error mechanism can be reduced by many orders of magnitude. I also comment on how this affects other solid-state qubits.

Quantum computers are proposed to perform calculations that cannot be run by classical supercomputers, such as efficient prime factorization or solving how molecules bind using quantum chemistry [1, 2]. Such difficult problems can only be solved by embedding the algorithm in a large quantum computer that is running quantum error correction.

Quantum computers have intrinsic errors, so algorithms can be natively run with typically only a few hundred to thousand logic operations [3, 4]. In order to run the most powerful and useful algorithms, say with millions to billions of logic gates, errors must be reduced to a parts per million or billion range, or lower. Fortunately, this is possible using quantum error correction, where the qubit state is distributed to many physical qubits in a way similar to classical error correction, so that errors in the physical qubit states can be selectively measured, decoded and corrected. For example, surface code error correction encodes a protected “logical” state with about 1000 physical qubits [5, 6]. As long as physical errors are small, about 0.1%, and occur randomly and independently among these 1000 qubits, then the logical error can be less than 0.1 part per billion [7]. However, if errors are large or correlated, bunching together either in time or across the chip in space, then error decoding fails. With a logical error, the memory of the quantum computer is lost and the algorithm fails.

This paper explains how cosmic rays and background gamma ray radiation are pulsed energy sources that produce large and correlated errors in superconducting qubits. Cosmic rays naturally occur from high energy particles impinging from space to the atmosphere, where they are converted into muon particles that deeply penetrate all matter on the surface of the earth. When the muons traverse the quantum chip, they deposit a large amount of energy in the substrate of the quantum processor, on average 460 keV [8], which then briefly “heats” the chip. Gamma rays from natural background sources have a somewhat larger rate and can deposit even greater energy, up to about 1 MeV [8]. Experiments on low-

temperature detectors and qubits have observed such radiation [8–14].

A model is presented here that quantitatively describes the phonon down-conversion process to quasiparticles, which then decays the qubit state. This model shows that greater than 90% of the radiation energy is converted into phonons [8, 15]. For present designs, the model predicts 57% of the phonon energy then breaks Cooper pairs with significant consequences: these quasiparticles reduce the qubit energy decay rate $1/T_1$ to the range of 1/16-1600 ns [16, 17], they have a large spatial extend of mm to cm range, they have a long duration of 100 μ s to 10 ms, and they occur more than once per minute. Each of these parameters is troubling, but in combination they are large enough to kill a complex quantum computation by many orders of magnitude.

Using a quantitative model for the generation of quasiparticles and their decay, I show that one can reliably redesign the quantum processor by channeling the phonon energy away from the qubits. The most important change is using thick films of a normal metal or low-gap superconductor to channel energy away from qubits. This redesign should reduce the initial quasiparticle density by a factor of 100, usefully larger than for a previous detector experiment with thin films [11]. This work is also complementary to a recent paper that describes well the radiation physics and the effects of breaking electron-hole pairs in the silicon crystal as part of the down-conversion process [8]; such charge offsets should not be an issue with large transmon qubits [18].

PHONON DOWN-CONVERSION TO QUASIPARTICLES

At low temperatures the physics of thermalization often becomes slow, and sometimes the riskiest assumption is that a system can be simply described by a temperature. For the non-equilibrium physics described here, it is better to represent the system being mostly at a background temperature T , but with a small number of ex-

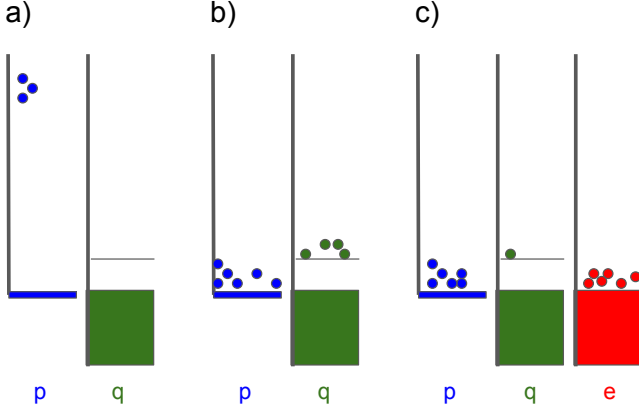


Figure 1. **Non-equilibrium phonon, quasiparticle and electron excitations.** a) Schematic representation of the phonon (p) and quasiparticle (q) excitations after the radiation event, with only a few high-energy phonons. The vertical axis represents the state energy. b) After relaxation, the phonon energy has down-converted to quasiparticle excitations in the superconductor and low-energy (sub-gap) phonons. About 57% of the initial energy remains in the quasiparticles. c) With a normal metal structure, most of the energy has been channeled away from the superconductor and towards the normal metal electrons (e), which is designed not to affect the qubit.

citations that can each be described by their energy E , their spectrum dn/dE , or the density of superconducting quasiparticles n_{qp} near the gap Δ . The basic idea is illustrated in Figure 1, where after the radiation event (a) there are a few high-energy phonons, which then get down-converted over time (b) to a larger number of low-energy phonons and quasiparticles. The quasiparticles radiate phonons until they are at the superconducting gap edge, where they slowly recombine over a $\gtrsim 100 \mu\text{s}$ time scale [17]. In the two-fluid model of a superconductor, the quasiparticles damp the qubit like a low density normal metal, with a superconducting qubit quality factor given by [16]

$$1/Q \simeq 1.23 n_{qp}/n_{cp} \quad (1)$$

where $n_{cp} = 2.8 \cdot 10^6 / \mu\text{m}^3$ is the density of Cooper pairs for aluminum, and the numerical factor is computed for 5 GHz. As plotted in the appendix, the decay rate is only weakly dependent on the energy spectrum of quasiparticles. We eventually want the excitations to be channeled to the normal metal and away from the qubit superconductor, as shown in Fig. 1(c).

The initial interaction of the radiation produces silicon electron-hole pairs and high-energy phonons up to the Debye energy 450 K [8]. These phonons down-convert to lower energy phonons, but this process stops at low energy where the phonon dispersion relationship becomes linear. Most of the electron-hole pairs recombine rapidly (ns time scales), with less than 10% of the radiation en-

ergy contributing to their net occupation [8, 15].

The down-conversion process for the phonon energy is a cascade of phonon and electron/quasiparticle scattering processes. Here, a high-energy phonon is converted to electron/quasiparticle pairs, which then scatters again to produce another lower-energy phonon. The relevant scattering processes are listed in Table I. These down-conversion processes are described by Kaplan *et. al.* for superconductors [19], but can also be used for normal metals by setting the gap to zero. As these rates are written as integrals over the Fermi occupation factors, the formulas can thus be rewritten to express a single-particle scattering rate versus energy.

The phonon energy E_p must be greater than 2Δ to produce two quasiparticles; the excess energy is split randomly between them, on average $E_q = \Delta + (E_p - 2\Delta)/2$. Similarly for quasiparticle scattering, the excess quasiparticle energy is distributed between the quasiparticle and phonon; because the phonon density of states scales as the square of frequency, on average the resulting phonon takes most of the energy $(3/4)(E_q - \Delta)$. The last scattering process in the Table is recombination, but since it scales as quasiparticle density the rate is small and can be ignored during the initial down-conversion cascade.

Electron-electron scattering is thought to be unimportant as its rate ($\sim E_e$) becomes relatively small compared to phonon scattering ($\sim E_e^3$) at energies above a few Kelvin. Also, retaining more energy in the electrons will not change significantly the results here.

The Table also lists scattering rates based on the power transfer between electrons and phonons, which can be directly measured in experiments. The power exchange between electrons and phonons within a volume V is given by [20]

$$P_{ep} = \Sigma V (T_e^5 - T_p^5), \quad (2)$$

which looks like the Stefan-Boltzmann radiation law, except here it describes the volume radiation of phonons. The materials constant Σ has been measured for elements

scattering	Kaplan	Power
p \rightarrow e + e	$(1/0.73 \text{ ns})(E_p/K)$	$(1/0.84 \text{ ns})(T_p/K)$
e \rightarrow e + p	$(1/400 \text{ ns})(E_e/K)^3$	$(1/0.25 \text{ ns})(T_e/K)^3$
p \rightarrow q + q	$(1.2/0.73 \text{ ns})(E_p/K)$	
q \rightarrow q + p	$(1/400 \text{ ns})((E_q - \Delta)/K)^3$	
q + q \rightarrow p	$(22/400 \text{ ns}) n_{qp}/n_{cp}$	

Table I. **Scattering processes.** Table of scattering processes for phonons (p), electrons (e) and quasiparticles (q), with initial energies E_p , E_e and E_q respectively. The “Kaplan” column represents the scattering rate given by reference [19], for aluminum. The “power” column is a rate from the power calculation given in the text, for copper. Both give estimates for scattering rates and their energy dependence.

and alloys Cu [20], Au [21], CuAu [22] and NiCr [23] and found to be reasonably constant $\Sigma \simeq 2 \text{ nW}/\mu\text{m}^3 \text{ K}^5$. For aluminum the value is about 10 times smaller [24], but the more widely-measured normal metal value will be used as an estimate. The total energies U of the electron and phonon systems are calculated by integrating heat capacities

$$U_p = (T_p^4/4) 6.7 \cdot 10^{-9} \text{ nJ}/\mu\text{m}^3/\text{K}^4 \quad (3)$$

$$U_e = (T_e^2/2) 9.8 \cdot 10^{-8} \text{ nJ}/\mu\text{m}^3/\text{K}^2, \quad (4)$$

where the estimated energies are for copper. Along with P_{ep} , approximate scattering rates are

$$\Gamma_p = P_{ep}/U_p \sim T_p \quad (5)$$

$$\Gamma_e = P_{ep}/U_e \sim T_e^3, \quad (6)$$

Note that the energy dependence for both the Kaplan and power formulas are the same.

For phonon scattering, the rates from the two estimates are quite close. However, the electron scattering rates differ by a large factor. The rate from the power formula should be more reliable since it is directly taken from power transfer experiments, as opposed to indirectly calculated from tunneling measurements. It turns out that the phonon rate is most critical for understanding the cascade, and that the electron rate only changes the scale of electron diffusion, which is not as critical when describing the cascade. For a conservative estimate, the slower Kaplan value is used here.

From these rates, a length scale for the cascade process can be estimated using the electron and phonon velocities. The results are summarized in Table II for a thin $0.1 \mu\text{m}$ aluminum film on a $400 \mu\text{m}$ thick silicon substrate. The most important length is for phonons, which shows that at an energy of 20 K, well above the superconducting gap for aluminum, the interaction length ($0.18 \mu\text{m}$) is somewhat larger than the film thickness ($0.1 \mu\text{m}$). This shows that a phonon in the aluminum will down-convert only a fraction of the time. The rest of the phonons escape the aluminum film, travel through the silicon wafer, and are then eventually reabsorbed after another impingement into the film. The probability of scattering lowers as the energy approaches $2\Delta = 4 \text{ K}$, so that the phonon on average will diffuse laterally by several thicknesses of the silicon substrate, of order a few mm's. The electrons in the metal, on the other hand, continue to move in the thin aluminum film and eventually down-convert after diffusing a much smaller distance 10 to $100 \mu\text{m}$.

PRESENT QUBIT DESIGN

Superconducting qubits are typically fabricated with superconducting metal fabricated on the surface of a silicon chip. To first calculate the efficiency of high-energy

Energy	e-rate	e-length	e-diffuse	p-rate	p-length
20 K	13/ns	$120 \mu\text{m}$	$3.5 \mu\text{m}$	25/ns	$0.18 \mu\text{m}$
4 K	0.01/ns	160 mm	$120 \mu\text{m}$	5/ns	$0.9 \mu\text{m}$

Table II. **Scattering lengths.** Table of electron (e-) and phonon (p-) scattering rates and lengths for an energy 20 K, well above the superconducting gap Δ of aluminum, and for $4 \text{ K} = 2\Delta$ at phonon freeze-out. Electron and phonon velocities are for copper $v_e = 1.6 \text{ mm/ns}$ and aluminum $v_p = 4.5 \mu\text{m/ns}$. The lengths are computed using these velocities, whereas the electron diffusion length also assumes diffuse scattering from a $0.1 \mu\text{m}$ thick Al metal film.

phonons being down-converted to quasiparticles, note that the scattering rates are not important. This is because high-energy phonons ($E_p > 2\Delta$) have to eventually scatter in the superconductor, and quasiparticles eventually have to scatter in the superconductor.

A numerical calculation of the down-conversion process uses the distribution of scattering energies discussed in the last section. The results are shown in Fig. 2, where the quasiparticle down-conversion efficiency $n_{qp}/(E_p/\Delta)$, which is normalized to the maximum possible number E_p/Δ , is plotted versus the initial phonon energy E_p/Δ . As expected, at low phonon energies $E_p < 2\Delta$, there is no breaking of Cooper pairs, but from $2\Delta < E_p < 4\Delta$ one quasiparticle pair is created. The numerical simulation shows that at larger phonon energies the average quasiparticle fraction is 0.57, which is reasonable since

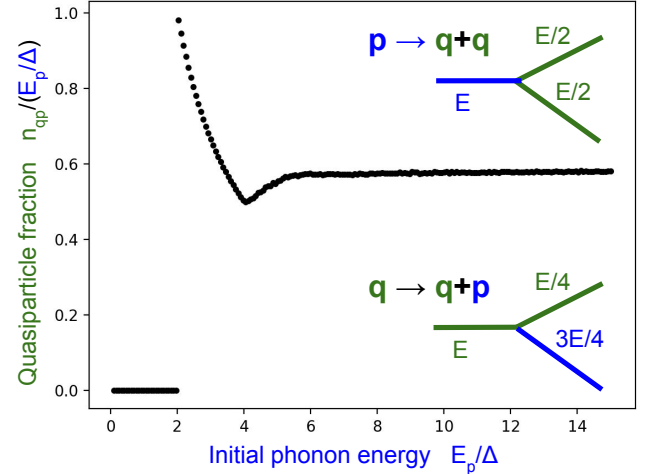


Figure 2. **Phonon to quasiparticle down-conversion efficiency.** Plot of normalized number of quasiparticles versus initial phonon energy, solved via numerical simulation for the random energy branching of the scattering processes $p \rightarrow q + q$ and $q \rightarrow q + p$. No quasiparticles are generated for $E_p < 2\Delta$, and 2 for $2\Delta < E_p < 4\Delta$, as expected. At high energies, 57% of the initial phonon energy is converted to quasiparticles on average. The insets depict the scattering process, listing the average final kinetic energies.

Initial radiation energy	0.2 MeV
Number of quasiparticles	$0.67 \cdot 10^9$
Density for $1 \text{ cm}^2 \times 0.1 \mu\text{m}$	$67/\mu\text{m}^2$
Density n_{qp}/n_{cp}	$2.4 \cdot 10^{-5}$
Qubit Q	51 k
T_1 for area 1 cm^2	$1.6 \mu\text{s}$
T_1 for 10 mm^2	160 ns
T_1 for 1 mm^2	16 ns

Table III. **Quasiparticle down-conversion and qubit decay.** Table of parameters for down-converting radiation energy into quasiparticles, which then damps the qubits. The aluminum film is assumed to be $0.1 \mu\text{m}$ thick over the entire 1 cm^2 chip. Also listed is T_1 for 2 smaller areas of the quasiparticle hotspot.

one expects the initial energy to be shared between both phonons and quasiparticles.

Assuming the qubits are embedded in a superconducting ground plane, typical for integrated circuits, these down-converted quasiparticles are expected to fill some area of the chip. The calculations for the down-conversion is show in Table III. An initial radiation energy is assumed to be 0.2 MeV, an typical value for muons and gamma rays. The next row is the number of quasiparticles using the aluminum gap and conversion efficiency 0.57. The quasiparticle density is next computed using a film thickness of $0.1 \mu\text{m}$ and a chip area of 1 cm^2 . Next is displayed the fraction density to Cooper pairs, and the estimated transmon quality factor Q . The computed $T_1 = 1.6 \mu\text{s}$ from Eq. (1) is short enough to significantly damp the qubit. As discussed previously, the initial hot-spot of the down-conversion is several times the silicon thickness, so an area of 10 mm^2 or even 1 mm^2 is more appropriate, in which case the decay times are severe, 160 ns to 16 ns respectively.

With an understanding of the basic scattering physics, the various stages of the energy down-conversion process are described next. We assume a low background temperature ($\sim 20 \text{ mK}$) well below the gap energy. The approximate time and length scales are included to estimate spatial and time correlations to the qubit error, along with the qubit decay T_1 to understand its magnitude.

1. Fireball: 10 ns, 0.5 mm. After a cosmic ray or gamma ray interacts with the substrate, high-energy phonons and silicon electron/holes are created. Most of the electron/holes recombine, placing greater than 90% of the initial energy into phonons. The phonon energy can down-convert by itself until about 20-40 K, when the phonon dispersion relation becomes linear. These phonons will spread through the substrate, moving laterally from the creation site. When impinging on the superconducting metal they will scatter with reasonably high probability ($\sim 50\%$) creating quasiparticles, so the

spatial extent of these excitations is approximately the substrate thickness.

2. Freeze out: 100 ns, 3 mm, $T_1 \simeq 160 \text{ ns}$. The quasiparticles and phonons continue to generate a cascade of scattering events, lowering the energy of the phonons until it drops below $2\Delta \simeq 4 \text{ K}$. At this time no additional quasiparticles are generated. About 57% of the initial energy is converted to quasiparticles. As shown in Table II, this time scale is set by the electron scattering rate, but the lateral extent is set by the phonon diffusion since the phonons typically impinge on the superconductor several times before absorption.

3. Qp diffusion: $100 \mu\text{s}$, 7 mm, $T_1 \simeq 1 \mu\text{s}$. At first the quasiparticles have energy somewhat larger than Δ , but now they shed their extra energy by emitting phonons. These phonons cannot be reabsorbed since they have energy below 2Δ , and thus bounce around the chip. The lateral growth of the quasiparticles are now set by their diffusion in the $0.1 \mu\text{m}$ film, with a distance D_q growing with time t as

$$D_q \simeq \sqrt{v_e t \cdot 0.1 \mu\text{m}} \quad (7)$$

$$= \sqrt{t/\mu\text{s}} \cdot 0.4 \text{ mm} . \quad (8)$$

At $100 \mu\text{s}$, they diffuse about 4 mm. This expanding area of quasiparticles decreases their density and increases the qubit T_1 approximately with t . Note that quasiparticles in the superconducting island of a differential transmon will not lower its density by diffusion, so the qubit decay rate $1/T_1$ may not lower over time except by recombination.

4. Qp recombination, and rebreaking: 1 ms, chip, $T_1 > 1.6 \mu\text{s}$. This stage is concurrent with the last stage of quasiparticle diffusion, but contains additional physics of quasiparticles recombining into Cooper pairs. Being a two-particle process, the rate is proportional to the quasiparticle density as given in Table I, which produces a density that decreases with time as [17]

$$\frac{n_{qp}}{n_{cp}} = \frac{400 \text{ ns}/43.6}{t - t_0} , \quad (9)$$

with $t_0 \sim 1 \text{ ms}$ for the density in Table III. Density does not decrease exponentially, so recombination is slow.

Additionally, after recombination the resulting phonon has no scattering mechanism other than re-breaking another Cooper pair. Thus the total number of quasiparticles is roughly constant in this stage. Here the phonons diffuse throughout the chip, so the re-created quasiparticles have roughly constant density. The qubit T_1 is now computed using the area of the substrate ground plane.

Quasiparticle recombination is more complicated because of trapping effects [25]. The quasiparticle density at the junction dominates qubit loss since the normal resistance of the junction is so much higher than

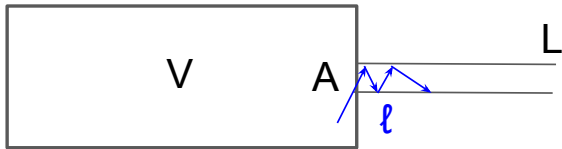


Figure 3. **Device schematic for phonon escape.** Phonons are uniformly moving in a substrate of volume V , and can escape through N_w wirebonds each with area A . The escape rate is proportional to the phonon velocity v_p . The phonons must diffuse down the wirebond, eventually escaping with a probability ℓ/L , where L is the wirebond length and ℓ is the mean free path taken as the wirebond diameter.

wiring. Quasiparticles will flow to and trap at the aluminum junction if its gap is less than the wiring and ground plane. Materials defects in the superconducting films can produce localized traps. Aluminum tends not to trap since scattering raises its transition temperature [26], whereas defects in niobium tend to lower its gap. Magnetic vortices also provide sites for lowering the gap for trapping [27].

5. Phonon escape: 4 ms, chip. The only mechanism for the 2Δ phonons to escape is by the connection to the copper chip mount, the thermal ground. Typically our chips are floating to reduce electromagnetic coupling, and only thermalized via wire bonds [28]. The physics for predicting the phonon escape rate is illustrated in Fig. 3, where the phonons are moving throughout the chip of volume V and can only escape through the N_w wirebonds each of area A . As they must diffuse down the wirebond of length L , the exit probability is ℓ/L , where ℓ is the mean free path, typically given by the diameter of the wire. The net phonon escape rate is

$$\Gamma_p = (N_w A/V) v_p (\ell/L). \quad (10)$$

This rate is $\Gamma_p = 1/4$ ms for parameters $N_w = 300$, $A = \pi(12\mu\text{m})^2$, $V = (10\text{mm})^2(0.4\text{mm})$, $\ell = 25\mu\text{m}$ and $L = 2\text{mm}$. At time scales much greater than $1/\Gamma_p$ all the phonons, both 2Δ and below, can escape and return the chip to thermal equilibrium.

It has been assumed here that the superconducting gap of the AlSi wirebonds is slightly higher than for the aluminum in the device, so that 2Δ phonons do not break Cooper pairs in the wirebonds. If they do, the quasiparticles will diffuse in the wirebond with an escape probability that is roughly equal to ℓ/L , making the above estimate still reasonable.

IMPROVED QUBIT DESIGN

The first priority when redesigning the qubit chip is to reduce the density of quasiparticles produced in the freeze-out stage. This can be readily done by adding a

normal metal to the substrate so that the phonon energy will be channeled to the normal metal, away from the superconductor. This normal metal also helps the stage of quasiparticle recombination and re-breaking, channeling the 2Δ phonons to the normal metal instead of back into the superconductor.

The effect of the normal metal can be numerically simulated with a similar method as used for Fig. 2, except a fraction of the phonon down-conversion is for electron excitations, not just quasiparticles. Here the fraction is estimated from the relative thicknesses for the superconducting and normal films because the electron-phonon interaction is roughly equal for many metals. As there are no direct measurements available now, this should give a good starting point for the design.

Figure 4 shows the simulation data for the quasiparticle fraction of down-conversion, plotted as the relative thicknesses of the superconducting (t_s) and normal (t_n) metal. The participation ratio $t_s/(t_s + 1.65 t_n)$ is chosen with the constant 1.65 so that the data lies on a line. This data shows that as the fraction of superconducting metal decreases, so does its fraction of quasiparticles from phonon down-conversion, as expected. Choosing the thickness of the normal metal will ultimately be optimized from experimental measurements of T_1 , but from the above estimates a decrease in quasiparticle density of 100 is likely needed, suggesting a thickness of $10\mu\text{m}$. This is significantly thicker than standard thin-film deposition techniques, so an electro-deposited copper, silver or gold film is most likely the best solution. These metals also have the advantage of low stress.

The natural placement of this normal metal film is the backside of the qubit substrate. However, such a design has problems with electromagnetic radiation. Figure 5(a) illustrates the idea with a simplified schematic of the design. A differential transmon qubit typically is embedded in a ground plane, so that the normal metal on the backside of the substrate forms a transmission line with low impedance, estimated to be $\sim 6\Omega$. The pads of transmon capacitor have an area of about 0.1mm^2 which form parallel plate capacitors that drive the transmission line mode. Since these capacitors are about 20% of the capacitance of the transmon, the qubit and transmission line are strongly coupled, so one expects a large effect on the transmon. This can be estimated by considering the equivalent circuit of Fig. 5(b), where the short transmission line between the capacitors is equivalently a $\sim 0.3\text{nH}$ inductor, with an impedance of 10Ω at 5GHz . This has a small effect on the equivalent resistance (6Ω) representing the transmission line radiation. The effect of the coupling and this resistor is to significantly damp the qubit with $Q \sim 1\text{k}$. Note that with strong coupling, this design will not work with any reasonable change to the transmission line impedance.

A straightforward solution is to break up the normal metal into isolated islands so that the small capacitance

between the islands stops the transmission line radiation. As this only modestly decreases the volume of the normal metal, the thermalization physics will not change much. For this design the equivalent circuit is given by Fig. 5(b) but with the resistance given by that across the copper island $\sim 0.01 \Omega$. For this low resistance the qubit will be lightly damped with $Q \sim 3$ M. If a higher Q is needed, an improvement would be to deposit a thin superconducting film between the substrate and the normal metal, for example titanium.

An alternative design would be to use a continuous superconducting ground plane on the backside, with many via connections to the qubit ground plane to short the transmission line mode. Then a continuous normal metal film could be used on the backside. The chip could even be placed on a copper mount with vacuum grease to better connect the substrate to thermal ground.

There is a remaining serious problem: quasiparticles that have been created still have a recombination time that is much longer than the error correction cycle ($\sim 1 \mu\text{s}$), creating errors correlated in time. This time can be estimated based on Eq. (9), which for a qubit $Q = 1$ M would require a time to decay $t - t_0 \sim 10$ ms. This is clearly too long, even if there is some other mechanism that decays the quasiparticles 10 to 100 times faster.

The solution is to build quasiparticle traps into the qubit layer [29, 30], so that any quasiparticles near the Josephson junction can diffuse into a lower-gap superconductor, relax its energy by the emission of a phonon, and thus be trapped away from the junction. Here I propose

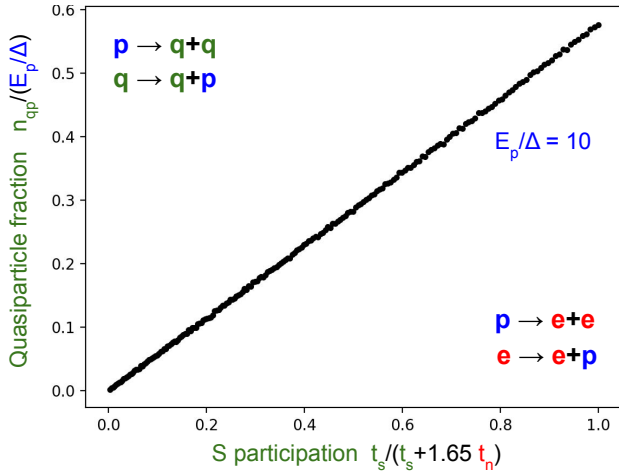


Figure 4. Reduction of quasiparticles from channeling energy to normal metal. Plot of normalized number of quasiparticles versus participation of the superconductor, showing the reduction of quasiparticles using normal metal. The participation formula is expressed with the thickness of the superconductor t_s and normal t_n metal, fitting the constant 1.65 to give a linear dependence. The initial phonon energy is $E_p/\Delta = 10$. The insets show the 4 scattering processes for the superconductor and the normal metal.

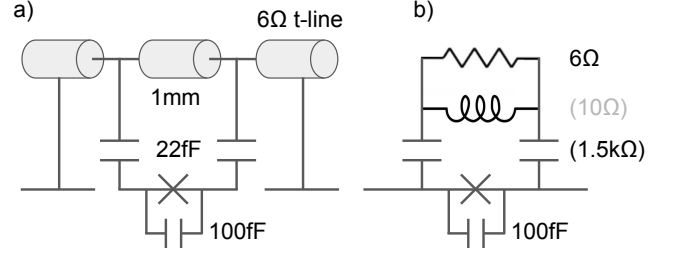


Figure 5. Equivalent circuit with backside metal. a) Circuit showing differential transmon embedded in a ground plane on the qubit layer. The continuous normal metal on the backside then acts as a low impedance transmission line of $\sim 6 \Omega$ impedance, which couples to the transmon via parallel plate capacitors coming from the qubit pads that have an area about 0.1 mm^2 . b) Simplified circuit, replacing the transmission line with an equivalent resistor, and the short transmission line between capacitors with an inductor, with impedances at 5 GHz shown in parenthesis. This heavily damps the qubit with a $Q \sim 1$ k.

making the traps large, covering most of the superconducting layer, so that quasiparticles are efficiently and quickly down-converted. The simple solution is to make the qubit wiring and ground plane out of a lower gap superconductor than for the aluminum junctions. For example, if the transition temperature was 0.5 K, then quasiparticles would quickly down-convert to the lower gap, creating a sufficient barrier for them to enter the junction superconductor. The wire superconducting gap would still be high enough to ensure little dissipation.

Other systems constraints might prevail for the wiring and ground, like choosing superconductors with small surface loss. In this case, quasiparticle traps could be used as illustrated in Fig. 6. Here a lower gap superconductor, as discussed above, is placed on the wiring and

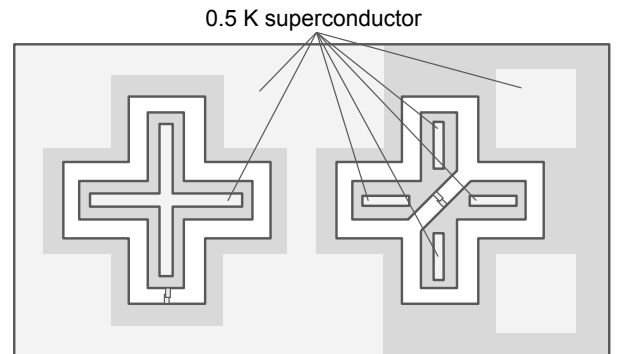


Figure 6. Design of quasiparticle traps. Illustration of quasiparticle traps for a Xmon (left) and differential transmon (right) where additional islands in the wiring and ground planes are made from a lower-gap superconductor. These islands can be directly connected to the wiring or through a thin tunnel barrier.

ground planes, close enough to all the metal so that quasiparticles will rapidly diffuse to the traps. The trap can be fabricated on top of the superconductor or by first growing a small tunnel barrier. From Table II, quasiparticles are estimated to diffuse for about 100 ns and $100\ \mu\text{m}$ before losing energy by shedding a phonon, and thus trapping. The thickness of the lower gap superconductor should be about the thickness of the wire and ground superconductor for efficient channeling of the energy.

For this improved design, the stages of energy decay should be the following.

1. Fireball: 10 ns, 0.5 mm. The initial cascade will have less diffusion laterally because the electron-phonon cascade can down-convert efficiently in the thick normal metal layer.

2. Freeze out: 100 ns, 2 mm, $T_1 \simeq 8\ \mu\text{s}$. About 99% of the phonon energy will be down-converted in the normal metal. Most phonons will not escape this layer even as their energy drops below 1 K. Some phonons escaping into the silicon and superconductor may diffuse laterally, but less than for the original design. Before the quasiparticle energy in the superconductor relaxes to the gap, the quasiparticle density at the junctions is estimated from the energy partitioning.

3. Qp diffusion and down-conversion: 200 ns, 2 mm, $T_1 \gg 8\ \mu\text{s}$. The quasiparticles at the junction should diffuse rapidly into the superconductor wiring. Because the distance to the low-gap superconductor islands is less than $100\ \mu\text{m}$, the diffusion time to the traps is short $< 100\ \text{ns}$. The down-conversion time once in the 0.5 K superconductor is about 200 ns. The T_1 of the qubit should reset to its background rate during this time.

4. Qp recombination: 1 ms, chip. During this time, all of the quasiparticles are in the low-gap superconductor, and will recombine over a long time scale as discussed previously. They should have little effect on the qubit because they are not in the junction, nor in the critical edges of the superconducting wiring or ground plane. Phonons created by recombination will be absorbed by the normal metal.

5. Phonon escape: 4 ms, chip. Phonons continue down-conversion in the normal metal and eventually escape to the copper chip mount.

A summary of the stages and a comparison between the present and future design is shown in Table IV.

The qubit lifetime is reduced for a time less than one surface code cycle. Qubit errors will be small and weakly correlated in space, maybe over one adjacent qubit. Error correction thus should work properly.

As a side benefit, note that surface loss is presently a dominant damping mechanism, coming from two-level states in surface oxides. They are likely producing the 0.1-1% thermal population observed in the qubit excited state, as the two-level states can be excited by non-equilibrium phonons at a frequency $\sim 5\ \text{GHz}$. Strong

stage	present			future		
	time (μs)	size (mm)	T_1 (μs)	time (μs)	size (mm)	T_1 (μs)
1. Fireball	0.01	0.5		0.01	0.5	
2. Freeze out	0.1	3	0.16	0.1	2	8
3. Qp diffusion	100	7	1	0.2	2	$\gg 8$
4. Qp recom. & rebrk.	1000	chip	> 1.6	1000	chip	bl
5. Phonon escape	4000	chip		4000	chip	bl

Table IV. **Summary of heating event.** For the 5 stages, the table summarizes the time scale, size scale, and qubit decay time. Shown is a comparison of present and improved design. The entry "bl" indicates T_1 decay approaches the baseline value.

down-conversion of phonons in the chip should reduce the effective temperature of these two-level-states and therefore the qubit.

OTHER QUBIT SYSTEMS

Cosmic rays and background gamma radiation is clearly important physics to understand in the systems design of a quantum computer. Although it has been discussed here in detail for superconducting transmon devices, this physics might be important for other low-temperature qubits. Here are some comments and questions:

For semiconductor qubits, the charge offsets produced by silicon electron-hole pairs [8] is as important as the phonon heating discussed here. This prior work shows that significant charge offsets would be seen over large areas ($100\ \mu\text{m}$) for charge-sensitive transmon devices. Will this introduce correlated qubit errors?

Photonic quantum computers are being designed based on superconducting transition detectors [31]. Might the phonon pulse described here be enough to trip these detectors in a way correlated in time and space, and thus detrimental to error correction?

Majorana qubits are made from a special quasiparticle state of a super- and semi-conductor. It would seem that one stray quasiparticle could disrupt this protected state [32]. Is it possible to reduce the quasiparticle number from billions to much less than one so that these states might stay protected?

More generally, will errors from radiation events disrupt any error-correction scheme that does not use many qubits to protect the state? Because radiation events produce non-equilibrium energy pulses of size about $100\ \mu\text{m}$, are large qubits necessary for errors not to be spatially correlated?

SUMMARY AND CONCLUSION

Research into thermal particle detectors has enabled low-temperature physicists to understand how radiation injects energy into quantum devices. The energy pulses from cosmic and gamma rays are clearly an important issue for superconducting qubits, since qubit errors and correlations in time and space will kill error correction by many orders of magnitude. A model is presented here for this physics, and a solution based on channeling this energy away from the qubit and into benign structures like thick normal metals and quasiparticle traps. There are many interesting experiments to do soon to demonstrate that an effective solution is possible.

I would like to thank R. McDermott for sharing a preprint before publication, and M. McEwen (a UCSB student working at Google) who shared initial experimental data and patiently waited for this publication.

Appendix

The appendix gives more detail on the rates. Figure 7 shows the dependence of the qubit energy loss $1/Q$ versus the energy of quasiparticles. Normally, the quasiparticles are near the gap, but in the freeze-out stage they are somewhat higher in energy.

Figures 8 and 9 show the rates of phonon decay and quasiparticle scattering, respectively, normalized to the rates for an equivalent metal that is in the normal state.

* martinis@quantala.tech

[1] P. W. Shor, Algorithmic Number Theory: First Inter-

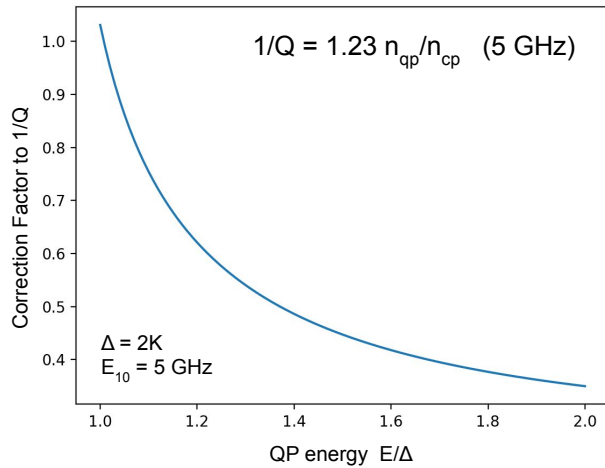


Figure 7. **Qubit decay rate.** Plot showing that the qubit decay rate can be lower when quasiparticles have not yet relaxed to the gap energy. From Eq. (3) of Ref. [16].

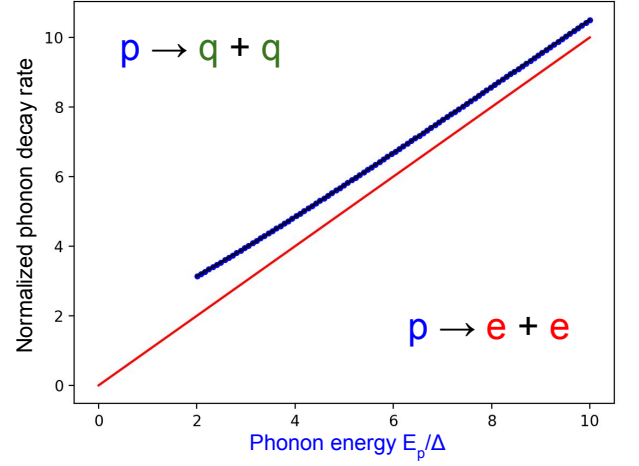


Figure 8. **Phonon decay rate.** Plot showing the phonon decay rate versus phonon energy (black dots), normalized to a normal metal (red line). No pair-breaking occurs below energy 2Δ , as expected. The normalized rate above 2Δ scales approximately as $E_p + 3.8\Delta/(E_p/\Delta + 2.5)^{0.8}$ (blue line). From Eq. (8) of Ref. [19].

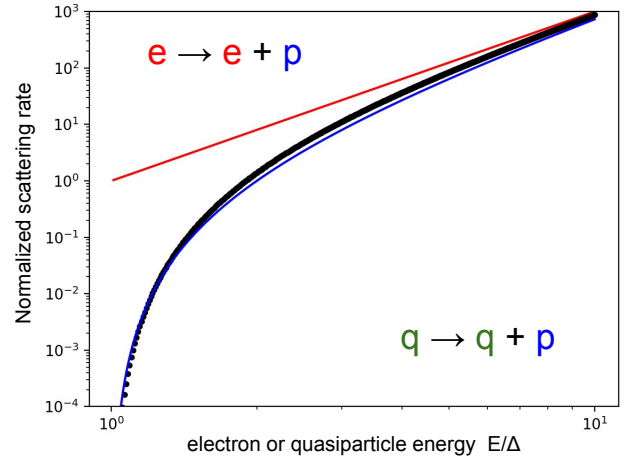


Figure 9. **Quasiparticle scattering rate.** Plot showing the quasiparticle decay rate versus energy (black dots), normalized to a normal metal (red line). The quasiparticle rate scales approximately as the final phonon density of states $(E_q - \Delta)^3$ (blue line). From Eq. (27) of Ref. [19].

- national Symposium, ANTS-I, Lecture Notes in Computer Science 877, edited by L. M. Adleman and M.-D. A. Huang (Springer, New York, 1994), p. 289.
- [2] D. W. Berry, C. Gidney, M. Motta, J. R. McClean, and R. Babbush, Qubitization of Arbitrary Basis Quantum Chemistry Leveraging Sparsity and Low Rank Factorization, *Quantum* **3**, 208 (2019).
 - [3] J. Preskill, Quantum computing in the NISQ era and beyond, *Quantum* **2**, 79 (2018).
 - [4] F. Arute *et al.*, Quantum supremacy using a programmable superconducting processor, *Nature* **574**, 505 (2019).
 - [5] S. B. Bravyi and A. Y. Kitaev, arXiv:quant-ph/9811052.

- [6] A. G. Fowler, M. Mariantoni, J. M. Martinis, and A. N. Cleland, Surface codes: Towards practical large-scale quantum computation, *Phys. Rev. A* **86**, 032324 (2012).
- [7] J. M. Martinis, Qubit metrology for building a fault-tolerant quantum computer, *NPJ Quantum Information* **1**, 15005 (2015).
- [8] R. McDermott, preprint.
- [9] K. D. Irwin, G. C. Hilton, D. A. Wollman, and J. M. Martinis, X-ray detection using a superconducting transition-edge sensor microcalorimeter with electrothermal feedback, *Appl. Phys. Lett.* **69**, 1945 (1996).
- [10] Grunhaupt *et al.*, Loss Mechanisms and Quasiparticle Dynamics in Superconducting Microwave Resonators Made of Thin-Film Granular Aluminum, *Phys. Rev. Lett.* **121**, 117001 (2018).
- [11] K. Karatsu *et al.*, Mitigation of cosmic ray effect on microwave kinetic inductance detector arrays, *Appl. Phys. Lett.* **114**, 032601 (2019).
- [12] Cardani *et al.*, Reducing the impact of radioactivity on quantum circuits in a deep-underground facility, arXiv:2005.02286.
- [13] A. P. Vepsäläinen *et al.*, Impact of Ionizing radiation on superconducting qubit coherence, *Nature* **584**, 551 (2020).
- [14] M. McEwen, private communication.
- [15] T. Shutt *et al.*, Simultaneous high resolution measurement of phonons and ionization created by particle interactions in a 60 g germanium crystal at 25 mK, *Phys. Rev. Lett.* **69**, 3531 (1992).
- [16] J. M. Martinis, M. Ansmann, and J. Aumentado, Energy Decay in Superconducting Josephson-Junction Qubits from Nonequilibrium Quasiparticle Excitations, *Phys. Rev. Lett.* **103**, 097002 (2009).
- [17] M. Lenander *et al.*, Measurement of energy decay in superconducting qubits from nonequilibrium quasiparticles, *Phys. Rev. B* **84**, 024501 (2011).
- [18] J. Koch *et al.*, Charge-insensitive qubit design derived from the Cooper pair box, *Phys. Rev. A* **76**, 042319 (2007).
- [19] S. B. Kaplan *et al.*, Quasiparticle and phonon lifetimes in superconductors, *Phys. Rev. B* **14**, 4854 (1976).
- [20] M. L. Roukes, M. R. Freeman, R. S. Germain, R. C. Richardson, and M. B. Ketchen, Hot electrons and energy transport in metals at millikelvin temperatures, *Phys. Rev. Lett.* **55**, 422 (1985).
- [21] D. R. Schmidt, C. S. Yung, and A. N. Cleland, Temporal measurement of hot-electron relaxation in a phonon-cooled metal island, *Phys. Rev. B* **69**, 140301 (2004).
- [22] F. C. Wellstood, C. Urbina, and J. Clarke, Hot-electron effects in metals, *Phys. Rev. B* **49**, 5942 (1994).
- [23] J. M. Martinis, unpublished
- [24] R. L. Kautz, G. Zimmerli, and J. M. Martinis, Self-heating in the coulomb-blockade electrometer, *J. of Appl. Phys.* **73**, 2386 (1993).
- [25] J. Aumentado, M. W. Keller, J. M. Martinis, and M. H. Devoret, Nonequilibrium Quasiparticles and 2e Periodicity in Single-Cooper-Pair Transistors, *Phys. Rev. Lett.* **92**, 066802 (2004).
- [26] R. W. Cohen and B. Abeles, Superconductivity in Granular Aluminum films, *Phys. Rev.* **168** 144 (1968).
- [27] C. Wang *et al.*, Measurement and control of quasiparticle dynamics in a superconducting qubit, *Nature Comm.* **5**, 5836 (2014).
- [28] J. Wenner *et al.*, Wirebond crosstalk and cavity modes in large chip mounts for superconducting qubits, *Superconductor Science and Technology* **24**, 065001 (2011).
- [29] K.M. Lang, S. Nam, J. Aumentado, C. Urbina, and J.M. Martinis, Banishing quasiparticles from Josephson-junction qubits: why and how to do it, *IEEE Trans. Appl. Superconductivity* **13** 989 (2003).
- [30] R.-P. Riwar *et al.*, Normal-metal quasiparticle traps for superconducting qubits, *Phys. Rev. B* **94**, 104516 (2016).
- [31] A. Verevkin, J. Zhang, and R. Sobolewski, Detection efficiency of large-active-area NbN single-photon superconducting detectors in the ultraviolet to near-infrared range, *Appl. Phys. Lett.* **80**, 4687 (2002).
- [32] T. Karzig, W. S. Cole, D. I. Pikulin, Quasiparticle poisoning of Majorana qubits, arXiv:2004.01264.